GHI CORRELATIONS WITH DHI AND DNI AND THE
EFFECTS OF CLOUDINESS ON ONE-MINUTE DATA

Frank Vignola
Department of Physics
1274 – University of Oregon
Eugene, OR 97403-1274
e-mail: fev@uoregon.edu

ABSTRACT

The relationships between global, diffuse, and direct normal irradiance (GHI, DHI, and DNI respectively) have been the subject of numerous papers, and average correlations between the diffuse fraction and beam and the clearness index have been determined. This study examines the relationship by separating the cloudless periods and the cloudy periods. The relationship during cloudless skies is well defined and data points fall into a fairly narrow band. When clouds are present, the relationship becomes more complex. First, a method is developed to identify cloudy periods using only GHI data. This is done by correlating GHI with the cosine of the solar zenith angle on clear days and using the difference between the clear sky estimates and measured GHI to identify cloudy periods. Once the cloudy periods have been identified, the relationship between GHI and DNI for cloudy periods is studied.

1. INTRODUCTION

Resource assessment requires knowledge of the solar irradiance incident on a collector's surface. It is impractical to measure this for all possible tilts and orientations, so models have been created to estimate the incident solar radiation. These models utilize the direct normal irradiance (DNI) and diffuse horizontal irradiance (DHI) to estimate the total irradiance incident on the collector (GTI). Unfortunately there is a scarcity of DNI and DHI measurements and one often has to rely on total, or more commonly call global, solar radiation on a horizontal surface (GHI). There are probably at least 100 times as many stations measuring GHI as DNI and DHI. Therefore, to calculate solar radiation on a

tilted surface, one needs to determine DHI and DNI from GHI measurements.

The relationship between global and diffuse irradiance has been the subject of numerous papers [1,2]. Some of the original studies used DHI data from instruments shaded by a shadowband. A correction was needed to estimate the amount of diffuse irradiance blocked by the shadowband, and this correction has a large uncertainty which diminished the accuracy of the models. The advent of automatic trackers with the capability to measure diffuse irradiance utilizing a shade ball provided more accurate diffuse data. It was then discovered that the first class pyranometers used for the GHI and DHI measurements had a thermal offset that skewed the results. In addition, the cosine response of pyranometers used to measure global irradiance added systematic errors to the reference data. It turned out that the most accurate diffuse measurements are obtained from second class 'black and white' type pyranometers mounted on automatic trackers with shade disks or balls blocking direct sunlight. Calculating the GHI by multiplying the DNI times the cosine of solar zenith angle and then adding the DHI gives a better estimation of the GHI than using a pyranometer to directly measure the incident solar radiation.

This study examines the relationship between GHI and DHI and DNI irradiance. The goal is to characterize the relationship and develop methodologies that can be used to calculate DHI and DNI from GHI measurements. First, the data used in this study is described and then the relationship between GHI, DNI, and DHI is examined. The relationship between GHI and DNI is characterized using one-minute data. The one-minute GHI data is then examined to determine how they can be best be used to calculate DNI. One month of data is used to determine whether improved cal-

culations are possible to model DNI from GHI data. The results of the study are then discussed.

2. EXPERIMENTAL DATA

The DHI data in this study comes from a Schenk Star pyranometer mounted in a Schenk ventilator on an automatic tracker. The instrument is cleaned five times per week and the output is recorded by a Campbell Scientific CR 300 data logger. The Schenk Star pyranometer used here was calibrated against an Eppley AHF cavity radiometer for the DNI measurement and an Eppley Precision Spectral Radiometer (PSP), thermally adjusted, for the DHI measurement. The calibration accuracy at 45° is ±1% or ±2% at a 95% confidence level (see Fig.1). The DNI measurement is from a Kipp and Zonen CHP 1 pyrheliometer that has a ±0.7% uncertainty at the 95% confidence level. GHI values are calculated using Equation 1.

$$GHI = DNI \cdot \cos(sza) + DHI \qquad \text{Eqn. 1}$$

where sza is the solar zenith angle. The uncertainty of the calculated GHI is ±2% for cloudy skies and about ±1% for clear skies.

The data are one-minute data and hourly data can be obtained by summing over the appropriate time interval.

3. RELATIONSHIP BETWEEN GHI AND DHI AND DNI

Most studies of GHI divide the global irradiance by the corresponding global extraterrestrial irradiance. The normalized value is called the clearness index [k_t]. Use of the

Fig. 1: Calibration data for a Schenk Star pyranometer.

clearness index helps eliminate systematic variations of the GHI values over the day and over the year by taking into account some of the variation resulting from the changing solar angles over the day and over the year. The clearness index k_t will be used in lieu of GHI for parameterizing the relationship with DNI.

When it is completely cloudy, DHI values are equal to GHI values. The DHI increases along with GHI values until the clouds become spare, and then the diffuse values decrease. On very sunny days, the DHI values are typically between 10 and 20% of the GHI values. Therefore, there is not a one-to-one correspondence between DHI and GHI. To obtain a one-to-one correspondence, DHI is divided by GHI to yield the diffuse fraction. When it is cloudy, the diffuse fraction is near one because DHI is nearly equal to GHI. However, when GHI is large, DHI is small and the diffuse fraction is small. Fig. 2 is a plot of diffuse fraction verses the clearness index. The data under all weather conditions are plotted as black circles and clear sky data are
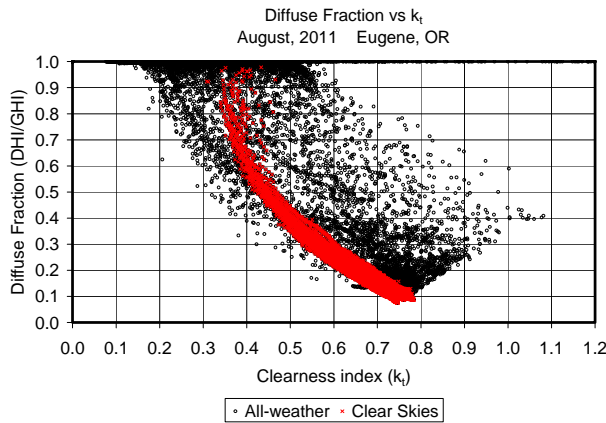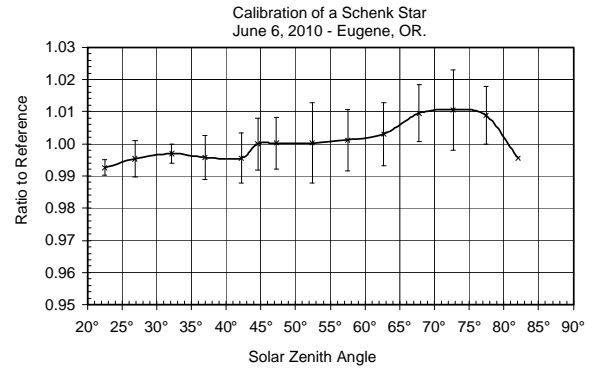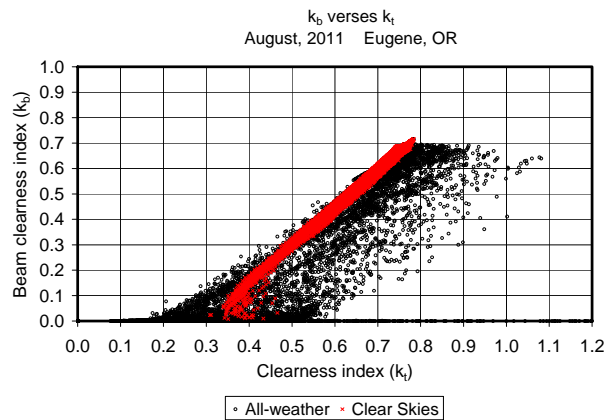

Fig. 2: Plot of diffuse fraction versus clearness index k_t using one-minute data. The black circles are all-weather conditions and the red 'x's are clear sky periods.

Fig. 3: Plot of k_b versus k_t using one-minute data. The black circles are all-weather conditions and the red 'x's are clear sky periods.

plotted as red x's. The clear sky values are clustered in a tight group on the left-hand side of the plot until k_t approaches a value of around 0.4. As k_t decreases from 0.4 to 0.375, the clear sky diffuse fraction increases from around 0.6 to 1. The data points that occur when the clear sky k_t values are below 0.4 occur in the early morning or late afternoon.

Note that there are some clearness index values greater than one. These values occur when there is a break in the clouds and the pyranometer receives direct sunlight and DNI irradiance is also reflected off nearby clouds onto the pyranometer. As the averaging time increase, to about 10 minutes, there are no longer k_t values greater than one. For hourly averaged data, the maximum value is about 0.8.

A complimentary relationship is between GHI parameterized as the clearness index (k_t) and the clearness index and the clearness index for direct normal beam irradiance (k_b) (Fig. 3).

$$k_b = DNI/DNI_{extraterrestrial} \qquad \text{Eqn. 2}$$

where $DNI_{extraterrestrial}$ is the extraterrestrial direct normal irradiance. Again the clear sky irradiance (the red 'x's in Fig. 3) is clustered on the left hand side of the plot. At a k_t of about 0.4, there is a steep decrease in k_b as k_t goes to its minimum clear sky value of around 0.375. This is similar characteristics as shown in Fig. 2 with the exception that for k_t values greater than 0.4 the relationship between clear sky k_b is almost a linear function of k_t. Therefore, it is deemed easier to work with the k_b k_t data than the diffuse fraction k_t data.

The relationship between clear sky GHI and k_b is depend-

ent on atmospheric aerosols. High quality clear sky models incorporate aerosols and this relationship varies over the year as the aerosol concentrations vary. Any relationship will have a seasonal dependence [3] and will change for areas with significantly different aerosol concentrations.

3.1 Extracting Information from GHI data

Usually only GHI values are available to obtain DNI and knowledge of the characteristics of the GHI data aids in obtaining the most accurate estimates of DNI. Again, the clearness index will be used, and k_t will be plotted against the cosine of the solar zenith angle (Fig. 4). The clear sky data are shown as red 'x's in Fig. 4 and fall in a tight band along the top of the data points. Therefore, one can then determine a clear sky formula relating k_t and the cos(sza).

For August, 2011 for Eugene, OR the clear sky relationship clearness index values can be obtained from by knowing the cosine of the solar zenith angle.

$$k_t = 0.3276 + 1.4194 \cdot x - 1.78262 \cdot x^2 + 0.836565 \cdot x^3 \quad \text{Eqn. 3}$$

where x is the cos(sza). The standard error for this fit is ± 0.0132. This demonstrates that a clear sky estimates of k_t can be obtained with a fair degree of accuracy with only knowledge of the time of day and hence the solar zenith angle.

For a comprehensive description of the k_t k_b relationship, it is necessary to account for the range of the k_b values observed in Fig. 3 for a give clearness index value. The correlation for clear-sky periods is straight-forward. For cloudy periods, the difference between the clear sky values
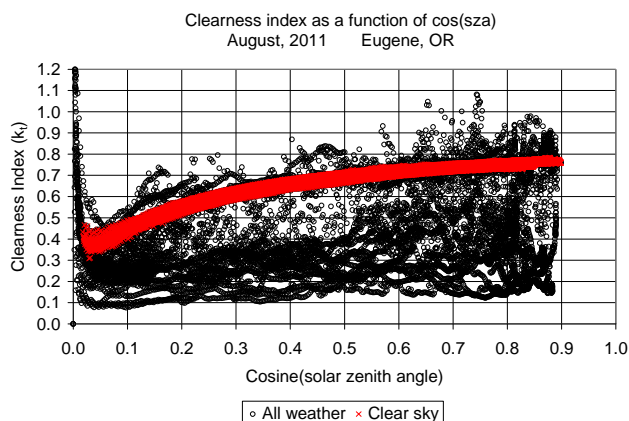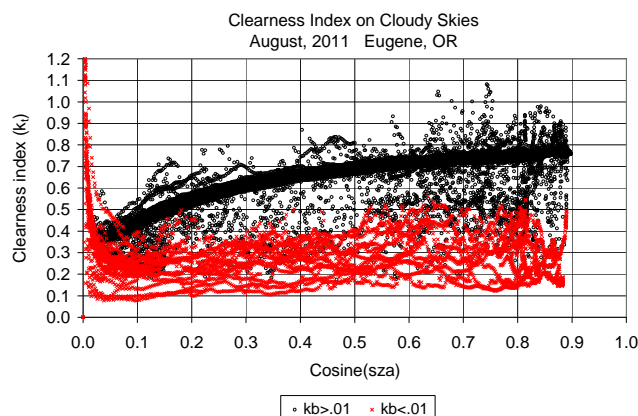

Fig. 4: Plot of clearness index versus cosine of the solar zenith angle. Data for all-weather conditions are plotted as black circles and clear sky data are shown as red 'x's.

Fig. 5: Plot of clearness index versus cosine of the solar zenith angle. Data are separated into cloudy and partially sunny or sunny periods. k_b less than 0.01 corresponds to DNI less than 14 W/m^2.

for a given clearness index and the actual value can be used as an indicator of the degree of cloudiness. This is useful information in developing a comprehensive relationship.

During period of total cloud cover, $k_b < 0.01$ is assumed here, there little or no direct sunlight. These data are all shown by the red 'x's on the lower part ($k_t < 0.3$) of the plot (Fig. 5). An exception occurs when the cosine of the solar zenith angle is very small. The points plotted on the left-hand side of Fig. 5 are associated with times having very small data values where uncertainties are approximately equal to the data values. These are the data points that would fall along the bottom axis of Fig. 3.

3.2 Clear Period Correlation

Using just the clear period data a simple correlation between k_b and k_t can be developed.

$$k_b = -0.8589 + 3.6578 \cdot k_t - 3.6220 \cdot k_t^2 + 1.9620 \cdot k_t^3 \quad \text{Eqn. 4}$$

The standard error for this is ±0.0123. As expected, just by identifying the clear sky periods for the GHI irradiance data, a very good correlation can be developed with k_b.

An alternative approach is to model the clear-period diffuse irradiance, Eqn. 1 can be used to obtain the correlation in the form of

$$k_b = k_t - a \cdot f(DHI)/GHI_{etr} \quad \text{Eqn. 5}$$

where f(DHI) is the function that describes DHI as a function of air mass (AM) or other parameters and GHI_{etr} is the extraterrestrial GHI value.

For August, 2011,

$$f(DHI)=326.25/AM -615.6/AM^2+676.3/AM^3-302.7/AM^4$$

and a = 0.9839.   Eqns. 6 a & b

This gives a slightly better description of k_b (see Fig. 6). A correlation with just k_t, such as that given in Eqn. 4, would produce a line in Fig. 6 because there is one value of k_b for each value of k_t. The correlation shown in Eqn. 5 is linear in k_t and also depends on a function of the inverse of air mass and the extraterrestrial GHI irradiance. The function f(DHI) matches the values of DHI best early and late in the day, and this time period is showing the widest range of possible k_b values near the bottom of Fig. 6.

To obtain an accurate model of clear sky DHI, information on the aerosol optical depth would be needed. Aerosols play an important role with any clear sky model and the correlation developed in August does not fit as well for other months with differing aerosol optical depths. For a comparison, Fig. 7 shows the clearness index plotted against the cosine of the solar zenith angle with December data. The estimated clear sky vales are plotted as red 'x's utilize the same correlation developed from August data (Eqn. 3) and result in estimated clear sky values that are about 7% lower than actual December values. The dark band above the red 'x's are measured December clear day values. The atmospheric aerosols for December are much reduced as compared to August in Eugene and this results in higher clear sky values. Therefore, to improve the clear sky portion of this model and to make the model more universal, inclusion of an aerosol optical depth factor is needed. In the appendix of an earlier work [4] a method is suggested that can incorporate aerosols. This method uses
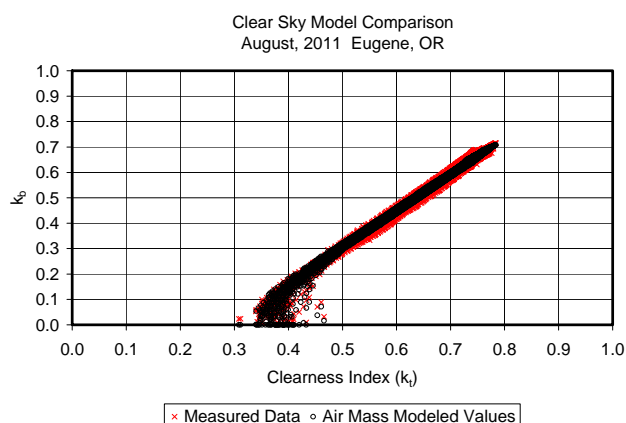

Fig. 6: Plot of measured clear sky data for August in Eugene, Oregon (red x's) plotted against modeled values, using Eqn. 4, that depend on air mass (black circles).
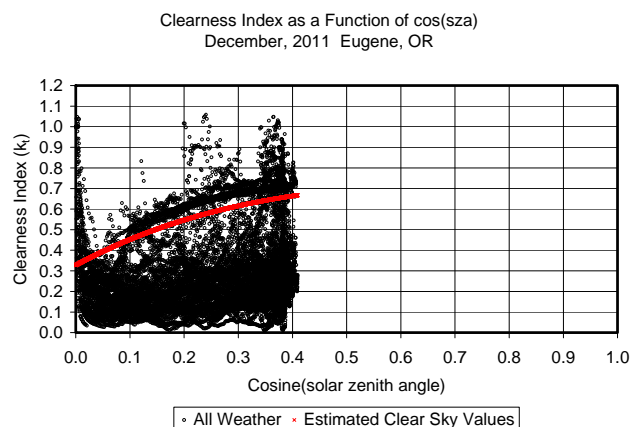

Fig. 7: Plot of clear sky model estimates (red 'x's) on top of the graph of clearness index plotted against cosine of the solar zenith angle for December 2011.

the work of Kasten and Young [5] and their Link turbidity factor. The Link turbidity factor incorporates aerosol information.

3.3 Separating Cloudy Data

Estimating k_b for partially-cloudy periods is more difficult than estimating k_b for clear periods. First, it is necessary to separate cloudy periods from clear-sky periods. Nearly every clear sky data point is within ±0.035 of the modeled clear sky values. Therefore a good starting assumption is that all data values within ±0.035 of the estimated clear sky value are clear sky value. However this assumption allows for cloudy sky values when the GHI values are changing rapidly and the values just happen to be near the clear sky values. The standard deviation of k_t over a three-minute period can be used to identify these data as coming from cloudy periods. This is shown in Fig. 8 that plots of the difference between measured clear sky k_b values and those calculated for clear sky periods. Data points shown as red 'x's have been identified by the standard deviation as coming from cloudy periods. Almost all of the data points in the plot that show a difference between measured and calculated clear sky k_b values greater than 0.1, occur when the standard deviation in the clearness index is greater than 0.01. Whereas the data in Fig. 6 was selected with a visual inspection of the data, the data in Fig. 8 what selected by the criterion that k_t was within ±0.035 of the clear sky global values. Using the standard deviation of the clearness index to eliminate cloudy periods results in a set of clear sky k_b values with a standard uncertainty of only ±0.015.

The cloudy sky data can be divided into several categories or conditions. First, in the cases where k_t is less than 0.2,

Fig. 8: Modeling the clear sky values of k_b. The black circles are for data where the standard deviation of the k_t is less than 0.01 and the red 'x's indicate a standard deviation of k_t greater than 0.01.

k_b is always very small. A correlation for this August data yields

$$k_b = 0.0145 \cdot k_t - 0.0016 \qquad \text{Eqn. 7}$$

A second category can be created when the cosine of the solar zenith angle is less than 0.1. A correlation can be created between the difference between k_t and k_b that is dependent on the difference between the calculated clear sky value of k_t and the measured value such that

$$k_t-k_b = 0.3417 - 0.7867*\Delta cs + 0.9799*\Delta cs^2 \qquad \text{Eqn. 8}$$

where Δcs is the difference between the calculated clear sky clearness index given in Eqn. 3 and the measured clearness index (k_t).

In Fig. 9 k_t-k_b is plotted against Δcs. While a correlation can be developed between k_t-k_b and the difference between the modeled clear sky values and measured clear sky index, the relationship only approximates the average relationship on average.

For $\Delta cs<0$,

$$k_t-k_b=0.1582-0.9263*\Delta cs+0.4277*StDev(k_t) \qquad \text{Eqn. 9}$$

where $StDev(k_t)$ is the standard deviation of the data from one minute before the specified time to one minute after it. Use of shorter time intervals seems to yield a better fit for the correlation results.

For $\Delta cs>0$,

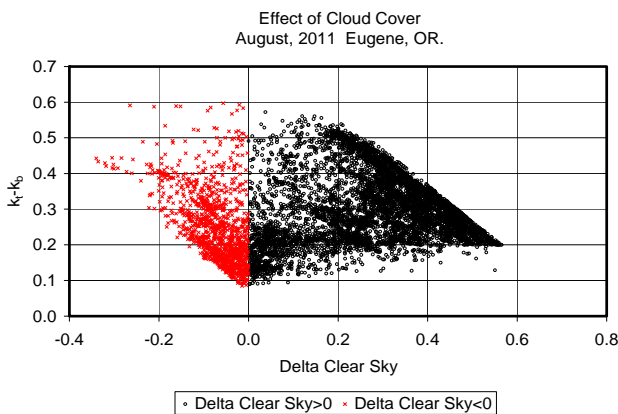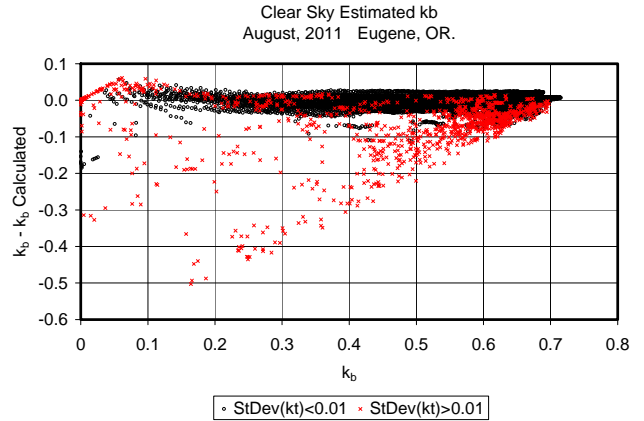$$k_t-k_b=0.1917+1.0651*\Delta cs-1.9666*\Delta cs^2 \qquad \text{Eqn. 10}$$

Fig. 9: Plot of cloudy period data for August 2011 in Eugene, OR against difference between clear sky model and measured k_t. Red 'x's are shown when k_t exceeds clear sky model values and black circles are shown when estimated clear sky values exceed measured k_t.

Correlation Results
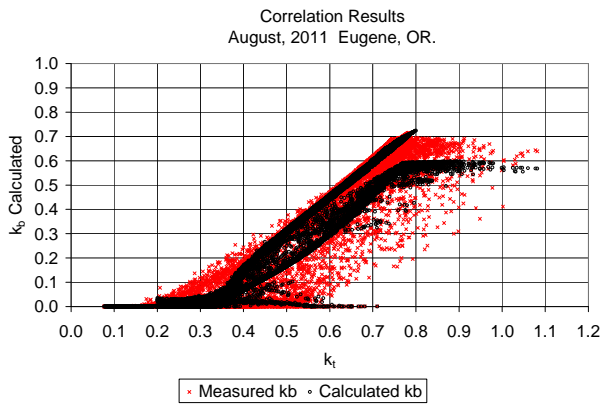August, 2011 Eugene, OR.

Fig. 10: Correlation results are compared with measured data. The red 'x's show the measured one minute data and the black circles show the estimated k_b values modeled from the measured GHI values.

These results are only derived for August 2011 in Eugene, Oregon.

The standard deviation for k_b during the cloudiest periods is ±0.07 while the overall standard deviation for all August data is closer to ±0.04. August is a fairly clear month in Eugene and the smaller overall standard deviation is indicative of the much better fit for clear sky periods.

4. CONCLUSIONS

A study of the relationship between the clearness index (k_t) and DNI clearness index (k_b) has been undertaken using one-minute August, 2011 data from Eugene, Oregon. The relationship has been broken down based on two conditions, a clear sky condition and a cloudy sky condition. A methodology for separating the clear sky and cloudy sky conditions has been demonstrated using only information provided by k_t and the variation of k_t over time.

The relationship between k_t and k_b during clear periods can be described with a reasonable of accuracy (a standard deviation of ±0.017). During cloudy periods the errors are about five times as large. A comparison between the modeled results and measured data is shown in Fig. 10. Some of the features of the k_t k_b relationship are accurately reproduced, especially for clear periods. For cloudy periods, while the average relationship is reproduced the actual distribution of the data points is not mimicked by the modeled data.

Dividing the relationship into clear and cloud periods is an improvement over a single formula relating k_b to a function of k_t. Future studies will attempt to incorporate the effects of aerosol optical depth into the relationships and delve deeper into methods to reproduce the distribution of data point for cloudy periods.

5. ACKNOWLEDMENTS

6. REFERENCES

[1] C.A. Gueymard and D.R. Myers. 2009. Evaluation of conventional and high-performance routine solar radiation measurements for improved solar resource, climatological trends, and radiative modeling. *Solar Energy,* vol. 83, 171-185.

[2] Randall, C. M. and J. M. Biddle. 1981. Hourly Estimates of Direct Insolation: Computer Code ADIPA User's Guide, The Aerospace Corporation, AIR-81 (7878)-1, September 1981.

[3] Vignola, F. and D. K. McDaniels, 1984. Diffuse-Global Correlations: Seasonal Variations, *Solar Energy*, 33, 397.

[4] Vignola, F. and D. K. McDaniels, 1988. Direct Beam Radiation: Projection on Tilted Surfaces, *Solar Energy* 40, 237.

[5] Kasten, F. and A. T. Young. 1989. Revised optical air mass tables and approximation formula. *Applied Optics* 28:4735–4738.